Proceedings of the ASME 2017 Conference on Smart Materials, Adaptive Structures and Intelligent Systems
SMASIS2017
September 18-20, 2017, Snowbird, UT, USA

SMASIS2017-3886

MULTIFUNCTIONAL NMC-SI BATTERIES WITH SELF-ACTUATION AND SELF-SENSING

Jun Ma
Mechatronics Research Laboratory
Department of Mechanical and Nuclear Engineering
The Pennsylvania State University
University Park, Pennsylvania 16802
Email: jxm1153@psu.edu

Christopher Rahn*
Professor
Mechatronics Research Laboratory
Department of Mechanical and Nuclear Engineering
The Pennsylvania State University
University Park, Pennsylvania 16802
Email: cdrahn@psu.edu

Mary Frecker
Professor
Department of Mechanical and Nuclear Engineering
The Pennsylvania State University
University Park, Pennsylvania 16802
Email: mxf36@engr.psu.edu

ABSTRACT

Among anode materials for lithium ion batteries, silicon (Si) is known for high theoretical capacity and low cost. Si changes volume by 300% *during cycling, however, often resulting in fast capacity fade. With sufficiently small Si particles in a flexible composite matrix, the cycle life of Si anodes can be extended. Si anodes also demonstrate stress-potential coupling where the open circuit voltage depends on applied stress. In this paper, we present a NMC-Si battery design, utilizing the undesired volume change of Si for actuation and the stress-potential coupling effect for sensing. The battery consists of one* $Li(Ni_{1/3}Mn_{1/3}Co_{1/3})O_2$ *(NMC) cathode in a separator pouch placed in an electrolyte-filled container with Si composite anode cantilevers. Models predict the shape of the cantilever as a function of battery state of charge (SOC) and the cell voltage as a function of distributed loading. Simulations of a copper current collector coated with Si active material show 11.05 mAh of energy storage, large displacement in a unimorph configuration (>60% of beam length) and over 100 mV of voltage change due to gravitational loading.*

*Address all correspondence to this author.

1 INTRODUCTION

Lithium ion batteries are widely used for high power and energy density applications such as portable devices, electric vehicles and drones [1] [2]. Among anode material candidates, Si has high theoretical capacity (4200 mAh/g [3] compared to graphite's 372 mAh/g [4]), making it an attractive option for high energy density batteries. Si anodes change volume by up to 300% when fully lithiated [5], indicating their potential as an actuator material. Si is as stiff as PZT but lithium actuation provides several orders of magnitude higher strain than PZT. Thus, the lithiated Si can provide high actuation energy density. Actuation bandwidth and fatigue, however, are limited due to slow diffusion dynamics and pulverization of the anode under high volume change. Using small Si particles (<100 nm) in a compliant, conductive matrix can improve diffusion rates and reduce cracking [6] [7]. Si anodes also demonstrate significant stress-potential coupling effect [8] [9] [10] so applied stress can significantly change the battery voltage, enabling a self-sensing battery design. Unlike actuation, the Larché-Cahn potential [11] [12] [13] developed due to applied stress is theoretically instantaneous so the sensing bandwidth could be quite high. In this paper, we demonstrate that a composite electrode consisting of Si particles and perfectly bonded binder single-side coated on a copper current collector can store energy, change

shape, and sense applied stress, as shown in Fig. 1. To analyze the energy storage, actuation, and sensing performance of this system, a stress-coupled, single-particle, electrochemical model and unimorph composite beam model are integrated to predict battery voltage and beam displacement, as functions of the charge/discharge current. Simulations demonstrate a multifunctional battery design that can store electrical energy, self-actuate through beam bending, and self-sense applied stresses.

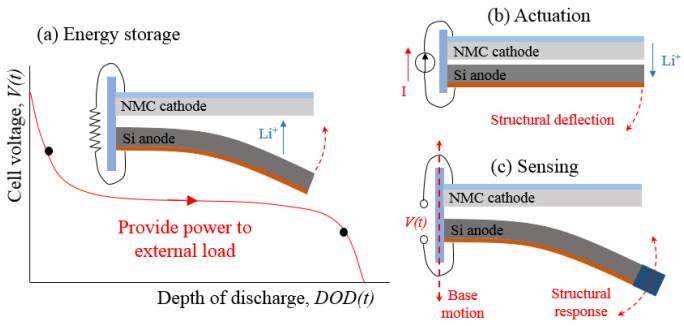

FIGURE 1. CONCEPT OF MULTIFUNCTIONAL BATTERY WITH SI COMPOSITE ANODE: (A) ENERGY STORAGE AND POWER SUPPLY TO EXTERNAL LOAD; (B) ACTUATION WITH STRUCTURAL DEFLECTION DURING CHARGING; (C) SENSING VIA VOLTAGE OUTPUT IN RESPONSE TO BASE MOTION

2 BATTERY DESIGN

Fig. 2 shows the proposed battery design. The battery consists of one NMC cathode and six Si anodes. To prepare the cathode, NMC particles are mixed with polyvinylidene fluoride (PVDF) binder and carbon black (CB) conductive additive in N-methyl-2-pyrrolidone (NMP) solution to form a uniform slurry. The slurry is then coated on Al current collector. When dried, the coating layer forms a porous structure. The Al current collector is connected to an Al wire. The cathode is encased in a polypropylene/polyethylene/polypropylene (PP/PE/PP) tri-layer separator pouch which allows Li ions travel through while providing electrical insulation. For the anodes, Si nanoparticles, polyacrylic acid (PAA) binder and CB conductive additive are dissolved in de-ionized water and then single-side coated on Cu current collector. The coated sides of the anodes face the cathode. One end of each anode is connected to a Cu wire. The wires are twisted together and insulated from each other, allowing measurement of individual anode potential. The other ends are attached to various sizes of Ni proof mass. The cathode and clamped ends of

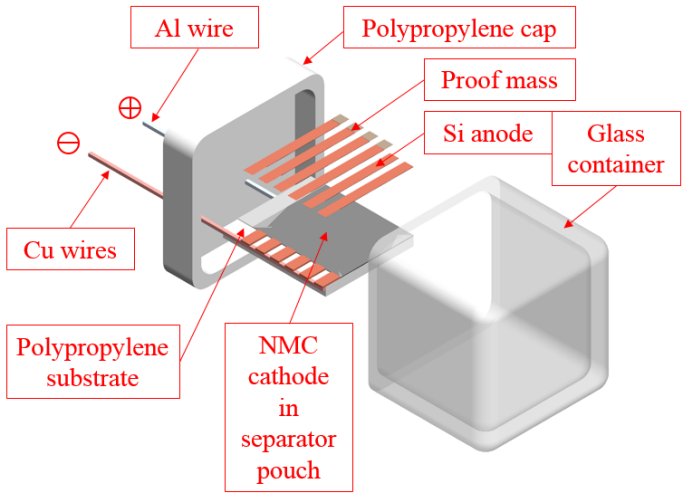

FIGURE 2. MULTIFUNCTIONAL NMC-SI BATTERY DESIGN

the anode cantilevers are attached to a PP substrate. This setup is installed in the cap of an optical grade glass chamber, with wires penetrating through sealed openings in the cap for electrical connections. The chamber is filled with electrolyte (1M $LiPF_6$ in EC/DMC/DEC solution). With this design, the anodes are free to deform inside the container and we are able to observe and measure electrode deflection and battery voltage from outside.

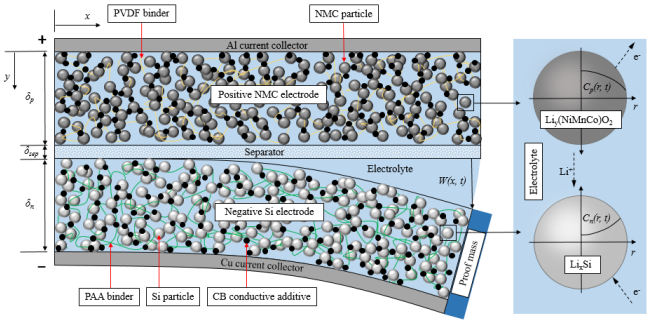

FIGURE 3. ELECTROCHEMICAL AND MECHANICAL MODEL

Fig. 3 shows a schematic diagram of the device model. The inputs are current and applied gravitational loading from the beam and proof mass. The outputs are battery voltage and negative electrode deformation. During charging, lithium ions migrate out of cathode particles, diffuse through separator and insert into anode particles. During discharge, lithium ions travel from the anode back to the cathode. The process involves com-

plex mass and charge transfer in porous media and through the solid-electrolyte interphase (SEI). Physically based, full order models are computationally complex and are difficult to parameterize. An often-used simplification of the full order model, the single particle model (SPM) [14] [15], assumes current input is distributed uniformly in each electrode so the electrode particles are connected in parallel. In this way, we use one spherical particle to represent each electrode. The electrolyte dynamics is simplified to internal resistance, by assuming instantaneous lithium ion diffusion in the liquid phase. This model has been proven to work sufficiently well for graphite electrodes under low C-rates [16]. For Si electrodes, the high volume change due to lithium insertion and applied loading can result in high stresses. The generated stress will then accelerate lithium transport, resulting in a electromechanical coupling phenomenon. Therefore, we utilize stress-coupled single particle model to predict device output.

3 SI SINGLE PARTICLE MODEL

3.1 Mechanical Equations

Following [17], the stress-strain relationship with an existing concentration gradient in the spherical Si particle is

$$\tilde{\varepsilon} = \frac{1}{E}\left[(1+\nu)\,\tilde{\sigma} - \nu\Theta\tilde{I}\right] + \frac{\Omega\bar{C}}{3}\tilde{I}, \tag{1}$$

where $\tilde{\varepsilon}$ is strain tensor, $\tilde{\sigma}$ is stress tensor, Θ is trace of $\tilde{\sigma}$, $\tilde{I}$ is 2^{nd} order unit tensor, E and ν are Young's modulus and Poisson's ratio, respectively, Ω is partial molar volume, $\bar{C} = C - C_0$ is the difference of lithium ion concentration C from its initial value C_0. The geometric equation

$$\tilde{\varepsilon} = \frac{1}{2}\left(\nabla\boldsymbol{u} + \boldsymbol{u}\nabla\right), \tag{2}$$

where $\boldsymbol{u}$ is the displacement vector. The equilibrium equation, neglecting body forces, is

$$\nabla\cdot\tilde{\sigma} = \mathbf{0}. \tag{3}$$

As a spherically symmetric problem, $\boldsymbol{u}$ only has a radial component u. $\tilde{\varepsilon}$ and $\tilde{\sigma}$ have radial (ε_r, σ_r) and tangential (ε_t, σ_t) components. Eqs. 1 2 3 simplify to

$$\begin{cases} \dfrac{du}{dr} = \dfrac{1}{E}\left(\sigma_r - 2\nu\sigma_t\right) + \dfrac{\Omega}{3}\bar{C} \\ \dfrac{u}{r} = \dfrac{1}{E}\left[\sigma_t - \nu\left(\sigma_r + \sigma_t\right)\right] + \dfrac{\Omega}{3}\bar{C} \end{cases} \tag{4}$$

and

$$\frac{d\sigma_r}{dr} + \frac{2}{r}\left(\sigma_r - \sigma_t\right) = 0. \tag{5}$$

The boundary conditions are

$$\begin{cases} u|_{r=0} = 0 \\ \sigma_r|_{r=r_0} = 0 \end{cases}, \tag{6}$$

where r_0 is particle radius. Substituting Eq. 4 into Eq. 5, we obtain the displacement equation

$$\frac{d^2u}{dr^2} + \frac{2}{r}\frac{du}{dr} - \frac{2u}{r^2} = \frac{1+\nu}{1-\nu}\frac{\Omega}{3}\frac{d\bar{C}}{dr}, \tag{7}$$

whose general solution

$$u = \frac{1+\nu}{1-\nu}\frac{\Omega}{3}\frac{1}{r^2}\int\bar{C}r^2dr + Ar + \frac{B}{r^2}, \tag{8}$$

where A and B are integral constants can be determined using boundary conditions to be

$$\begin{cases} A = \dfrac{2(1-2\nu)\Omega}{3(1-\nu)r_0^3}\displaystyle\int_0^{r_0}\bar{C}r^2dr \\ B = 0 \end{cases}. \tag{9}$$

Accordingly, we obtain the displacement

$$u = \frac{1+\nu}{1-\nu}\frac{\Omega}{3}\frac{1}{r^2}\int_0^r\bar{C}r^2dr + \frac{2(1-2\nu)\Omega}{3(1-\nu)}\frac{r}{r_0^3}\int_0^{r_0}\bar{C}r^2dr, \tag{10}$$

and stress components

$$\begin{cases} \sigma_r = \dfrac{2\Omega E}{3(1-\nu)}\left(\dfrac{1}{r_0^3}\displaystyle\int_0^{r_0}\bar{C}r^2dr - \dfrac{1}{r^3}\int_0^r\bar{C}r^2dr\right) \\ \sigma_t = \dfrac{\Omega E}{3(1-\nu)}\left(\dfrac{2}{r_0^3}\displaystyle\int_0^{r_0}\bar{C}r^2dr - \dfrac{1}{r^3}\int_0^r\bar{C}r^2dr - \bar{C}\right) \end{cases}. \tag{11}$$

3.2 Electrochemical Equations

The chemical potential gradient drives lithium ion movement. The velocity of lithium ions

$$\boldsymbol{v} = -M\nabla\mu, \tag{12}$$

where M is the mobility of lithium ions and μ is the chemical potential. The chemical potential in an ideal solid solution

$$\mu = \mu_0 + RTlnX - \Omega\sigma_h, \tag{13}$$

where μ_0 is the equilibrium chemical potential, R is the universal gas constant, T is absolute temperature, X is molar fraction of lithium ions and $\sigma_h = \Theta/3$ is hydrostatic stress. Accordingly, the lithium ion flux

$$\boldsymbol{J} = C\boldsymbol{v} = -CM\nabla\left(\mu_0 + RTlnX - \Omega\sigma_h\right). \tag{14}$$

Assuming isothermal conditions, the diffusion coefficient $D = MRT$, so the lithium ion flux

$$\boldsymbol{J} = -D\left(\nabla C - \frac{\Omega C}{RT}\nabla\sigma_h\right). \tag{15}$$

Conservation of mass yields

$$\frac{\partial C}{\partial t} + \nabla\cdot\boldsymbol{J} = 0, \tag{16}$$

Substituting Eq. 15 into Eq. 16, we obtain

$$\frac{\partial C}{\partial t} = D\left(\nabla^2 C - \frac{\Omega}{RT}\nabla C\cdot\nabla\sigma_h - \frac{\Omega C}{RT}\nabla^2\sigma_h\right). \tag{17}$$

For a spherical particle, Eq. 17 can be written as

$$\frac{\partial C}{\partial t} = D\left[\frac{\partial^2 C}{\partial r^2} + \frac{2}{r}\frac{\partial C}{\partial r} + \theta\left(\frac{\partial C}{\partial r}\right)^2 + \theta C\left(\frac{\partial^2 C}{\partial r^2} + \frac{2}{r}\frac{\partial C}{\partial r}\right)\right], \tag{18}$$

where

$$\theta = \frac{\Omega}{RT}\frac{2\Omega E}{9(1-\nu)}. \tag{19}$$

The initial condition

$$C|_{t=0} = C_0, \tag{20}$$

and boundary conditions

$$\begin{cases} \left.\dfrac{\partial C}{\partial r}\right|_{r=0} = 0 \\ -D(1+\theta C)\left.\dfrac{\partial C}{\partial r}\right|_{r=r_0} = \dfrac{j_s}{F} \end{cases}, \tag{21}$$

where j_s is particle surface current density and F is Faraday's constant. Overpotential η drives lithium ion flux through the solid-electrolyte interphase. It is determined by Butler-Volmer kinetics

$$j_s = a_s i_0\left[exp\left(\frac{\alpha_a F\eta}{RT}\right) - exp\left(-\frac{\alpha_c F\eta}{RT}\right)\right], \tag{22}$$

where a_s is the electrode particle specific area, i_0 is exchange current density and α_a and α_c are the anodic and cathodic transfer coefficients of electrode reaction. Finally, we obtain the NMC-Si battery voltage

$$V_{battery} = \phi^p(y) + \eta^p - \phi^n(x) - \eta^n - IR_{in}, \tag{23}$$

where ϕ^p and ϕ^n are open circuit potentials (OCP) of the positive and negative electrodes, respectively, and R_{in} is battery internal resistance. The open circuit potentials are usually fitted polynomials from experiment data, where $y = C^p\left(r_0^p, t\right)/C_{max}^p$ and $x = C^n\left(r_0^n, t\right)/C_{max}^n$ are the dimensionless concentration at particle surface. Eq. 18 is solved numerically with Crank-Nicolson implicit finite difference method.

4 SI UNIMORPH CANTILEVER MODEL

Fig. 4 shows a schematic diagram of the single-side coated Si anode. To calculate its deflection during lithiation/delithiation, we assume: (1) the coating layer is a continuous and uniform material, with properties independent of lithium concentration; (2) the coating layer is perfectly bounded to the current collector. Thus, the Si anode is modeled as unimorph cantilever [19].

To calculate anode deflection, one major challenge is to find the relationship between the Si particle expansion and the coating layer expansion. Due to porous composite structure of the coating layer, this relationship is not known analytically. An upper bound on the coating expansion would be to assume that Si expansion equals coating expansion. This assumes, however, that

TABLE 1. MODEL PARAMETERS OF NMC-SI MULTIFUNCTIONAL BATTERY [14] [15]

Parameter	NMC cathode	Separator	Si anode
Length, L (m)	3×10^{-2}	3×10^{-2}	3×10^{-2}
Width, W (m)	3×10^{-2}	3×10^{-2}	$3\times10^{-3}\,(6pcs)$
Coating thickness, h_{ct} (m)	36.55×10^{-6}	20×10^{-6}	40×10^{-6}
Current collector thickness, h_{cc} (m)	15×10^{-6}		20×10^{-6}
Particle radius, r_0 (m)	5×10^{-6}		500×10^{-9}
Porosity, χ_p	0.3	0.5	0.5
Active material volume fraction, χ_{am}	0.644		0.3
Maximum lithium ion concentration, C_{max} (mol/m^3)	51830		77787
Solid phase lithium diffusion coefficient, D (m^2/s)	2×10^{-14}		1×10^{-16} [18]
Stoichiometry at 0% SOC	0.955473		0.15
Stoichiometry at 100% SOC	0.359749		0.9727
Exchange current density, i_0 (A/m^2)	2		20
Charge transfer coefficient, $\alpha_a,\ \alpha_c$	0.5, 0.5		0.5, 0.5
Young's modulus, E (GPa)			90
Poisson's ratio, ν			0.28 [18]
Partial molar volume, Ω (m^3/mol)	0		2.2639×10^{-5}
Internal resistance, R_{in} $(\Omega\, m^2)$		6×10^{-4}	
Cathode open circuit potential, ϕ^p (V)	$-10.72y^4+23.88y^3-16.77y^2+2.595y+4.563$		
Anode open circuit potential, ϕ^n (V)	$1591.3x^{10}-5797.0x^9+7595.8x^8-3043.1x^7$ $-2484.7x^6+3520.5x^5-1792.7x^4+471.007x^3$ $-64.2527x^2+4.3176x+0.0807$		

the pores and relatively soft binder do not absorb any of this expansion. A lower bound on coating would be to assume that the initial expansion is absorbed by the pores and only expansion above/beyond pore volume would cause coating expansion. In this paper, we take the more conservative approach of the latter approximation which should under-predict cantilever displacement. Using the parameters in Table 1, Si volume is $0.3V_{ct}$ and void is $0.5V_{ct}$, where V_{ct} is the coating layer volume. When fully lithiated, Si volume becomes $0.96V_{ct}$. Assuming the voids are fully occupied after lithiation, the coating layer volume becomes $0.96V_{ct}+0.2Vct=1.16V_{ct}$. The maximum linear strain is 5%, and the coating layer axial strain due to lithium insertion

$$\varepsilon_{ct}=\beta\hat{C}_{avg}, \tag{24}$$

where $\beta=5\%$ is linear strain rate and $\hat{C}_{avg}$ is normalized average lithium concentration. The Young's modulus of the coating layer is estimated as 150 MPa [20].

4.1 Unimorph Cantilever Model

The unimorph equilibrium conditions

$$N_{ct}=N_{Cu}=N, \tag{25}$$

where N_{ct} and N_{Cu} are the axial forces of anode coating and the copper current collector, respectively. The moment balance

$$M_{ct}+M_{Cu}-M_g=\frac{N}{2}\left(h_{ct}+h_{Cu}\right), \tag{26}$$

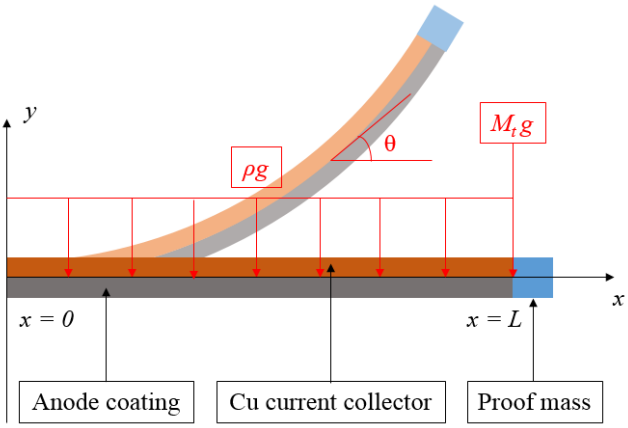

FIGURE 4. UNIMORPH CANTILEVER MODEL

where M_{ct} and M_{Cu} are the bending moments of the coating layer and copper layer (h_{ct} and h_{Cu} are their thicknesses), respectively. The gravitational moment

$$\begin{aligned} M_g &= -\int_0^{L-x} \rho g cos\theta x dx - M_t g cos\theta (L-x) \\ &= -\left[\frac{1}{2}\rho g (L-x)^2 + M_t g (L-x)\right] cos\theta, \end{aligned} \tag{27}$$

where ρ is the electrode linear density, M_t is the proof mass (assumed to be a point load at the end of the coating layer) and θ is the angle between the cantilever and horizontal. Assuming a linear cantilever bending moments-curvature (κ) relationship,

$$M_{ct} + M_{Cu} = \kappa (E_{ct} I_{ct} + E_{Cu} I_{Cu}), \tag{28}$$

where E_{ct} and E_{Cu} are Young's moduli and I_{ct} and I_{Cu} are cross-sectional moments of inertia of the coating layer and current collector, respectively. The non-slip interface condition can be written as

$$\beta \hat{C}_{avg} - \frac{N_{ct}}{E_{ct} A_{ct}} - \kappa \frac{h_{ct}}{2} = \frac{N_{Cu}}{E_{Cu} A_{Cu}} + \kappa \frac{h_{Cu}}{2}. \tag{29}$$

Combine Eqs. 26 27 28 29, we obtain the moment-curvature relationship

$$\kappa = \frac{2\beta \hat{C}_{avg} (h_{ct} + h_{Cu}) (E_{ct} A_{ct} + E_{Cu} A_{Cu}) + 4 M_g}{4 (E_{ct} I_{ct} + E_{Cu} I_{Cu}) + (h_{ct} + h_{Cu})^2 (E_{ct} A_{ct} + E_{Cu} A_{Cu})}. \tag{30}$$

4.2 Stress-Potential Coupling

The Larché-Cahn chemical potential [11] [12] [13] of lithium in solid solution

$$\phi_{Li} = \phi_{Li}^0 + RT log\left(\gamma \frac{C}{C_{max} - C}\right) - \frac{V_m \tau}{3}\Theta - \frac{V_m}{2}\tilde{\sigma} \cdot \tilde{\Xi} \cdot \tilde{\sigma}, \tag{31}$$

where ϕ_{Li}^0 is a reference chemical potential at $C = C_{max}/2$ and stress-free state, γ is the activity coefficient, τ is rate change of volumetric strain due to lithiation, V_m is electrode molar volume and $\tilde{\Xi} = d\tilde{S}/dC$, with $\tilde{S}$ being compliance tensor. Parameters V_m and $\tilde{\Xi}$ are unknown for composite porous electrodes, making it difficult to evaluate the stress-potential relationship analytically. Researchers found the stress-potential coupling for amorphous Si thin-films to be [9]

$$\frac{\Delta V}{\Delta \sigma} = 62\ mV/GPa, \tag{32}$$

indicating the Si potential decreases when compressed and increases when stretched. Thus, we substitute a simplified form of Eq. 31 into Eq. 23

$$V_{battery} = \phi^p(y) + \eta^p - \phi^n(x) - \eta^n - (62\ mV/GPa)\Delta\sigma - IR_{in}. \tag{33}$$

5 RESULTS

Fig. 5 shows the simulated response under a given current profile of constant current charging at 11.05 mA (1 C-rate, meaning an empty battery can be fully charged in 1 hour) for 3600 s, followed by constant current discharging at 11.05 mA for another 3600 s. Fig. 5(A) shows lithium ion distribution within a Si particle during charging. The particle develops a significant concentration variation from center to surface at the early stage of charging. Then the concentration gradient starts to decrease. Fig. 5(B) is battery voltage response to the current input. The voltage jumps suddenly when the current switches direction due to overpotential and internal resistance. The slope of the voltage response is primarily due to the slope of the OCP curves from Table 1. Fig. 5(C) shows the Si particle volume change as a function of time. When fully lithiated, the particle is 320% of its original size.

Fig. 6 shows the simulated Si anode shape change during charging. The beam is oriented vertically and deflects away from the cathode. In this orientation, gravitational loading has minimum effect on anode deformation so the proof mass contribution is neglected. Anode curvature increases with lithium concentration during charging, and decreases until reaching its original position during discharging. Unlike many smart material actu-

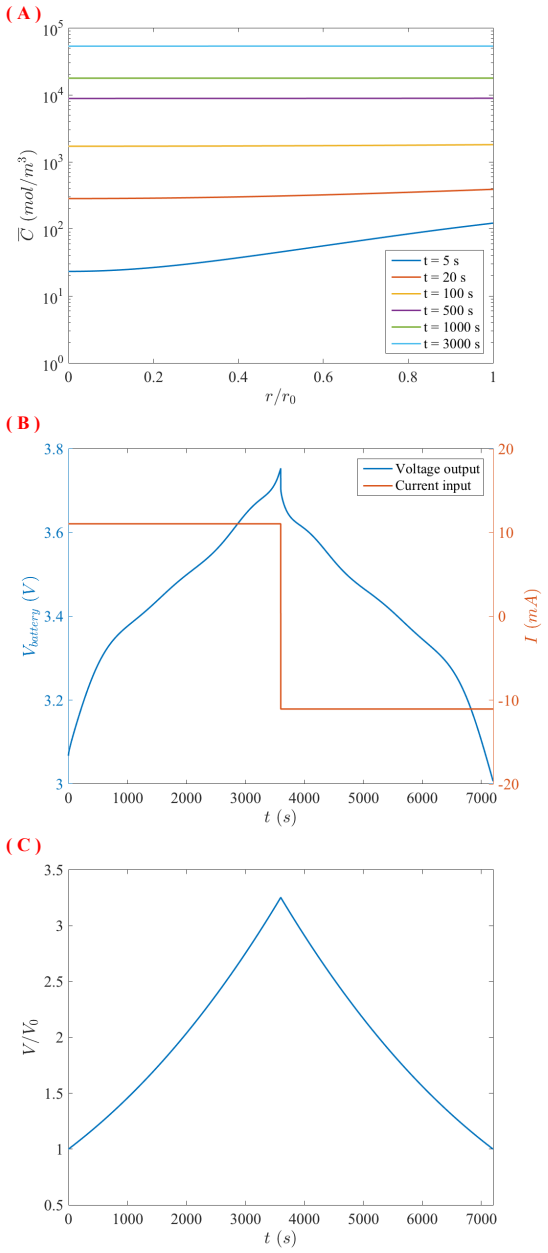

FIGURE 5. NMC-SI BATTERY SIMULATION RESULTS: (A) LI ION CONCENTRATION IN SI PARTICLE; (B) BATTERY CURRENT INPUT AND VOLTAGE OUTPUT; (C) SI PARTICLE VOLUME CHANGE.

ators, Si anode can hold its shape when disconnected from the power supply, due to low self-discharge of Li-ion batteries. The electrode design parameters such as coating composition, porosity and thickness ratio between coating and current collector can be tailored to provide the desired maximum displacement and blocked force.

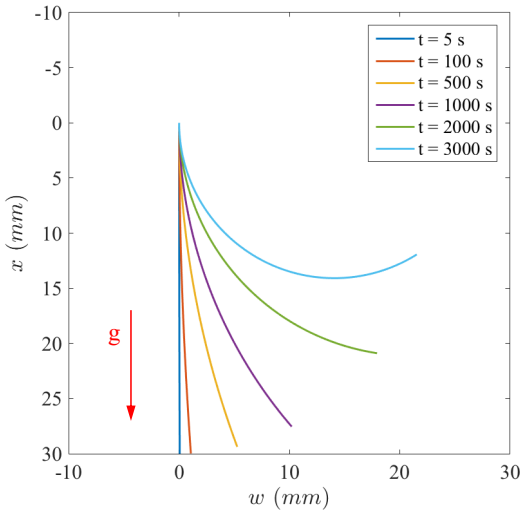

FIGURE 6. SIMULATED BATTERY ANODE DEFLECTION DURING LITHIUM INSERTION

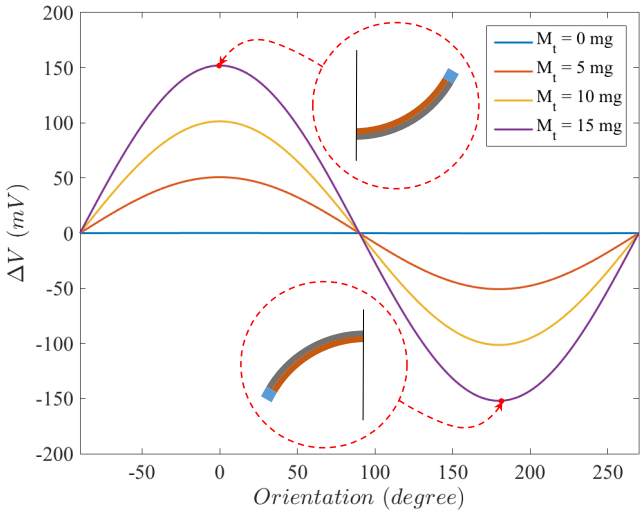

FIGURE 7. SIMULATED BATTERY VOLTAGE RESPONSE VERSUS BASE ROTATION

Fig. 7 shows the battery voltage response during base rotation. Starting vertically (-90°), the battery is rotated counterclockwise 360°. When the coating layer is above the current collector, the electrode is in compression, resulting in anode potential decrease and battery voltage increase. The battery voltage reaches its maximum at horizontal, when compressive stress peaks. When the coating is below current collector, the gravita-

tional moment stretches the coating layer, resulting in anode potential increase and battery voltage decrease. The battery voltage reaches its minimum at horizontal. The predicted voltage swing is large ($> 0.1\ V$) relative to the low noise floor typical of battery voltage measurement ($\sim 1\ mV$). This phenomenon is independent from battery state of charge. It is observed that the proof mass M_t plays an important role in determining voltage response range. Without proof mass, the voltage response range is only $0.24\ mV$. When the battery is used as an orientation sensor, the model can serve as a design guide to adjust sensitivity by tuning M_t.

6 CONCLUSIONS

This paper show that Si anodes and store energy, actuate through volume change associated with lithium insertion, and sense applied stress through stress-potential coupling. Simulations of a copper current collector coated with Si active material show 11.05 *mAh* of energy storage, large displacement in a unimorph configuration (>60% of beam length) and over 100 *mV* of voltage change due to gravitational loading.

REFERENCES

[1] Scrosati, B., Hassoun, J., and Sun, Y. K., 2011. "Lithium-ion batteries. a look into the future". *Energy & Environmental Science,* ***414***(6861), pp. 3287–3295.

[2] Kempton, W., 2004. "Electric vehicles: Driving range". *Nature Energy,* ***1***, p. 16131.

[3] Obrovac, M. N., and Christensen, L., 2004. "Structural changes in silicon anodes during lithium insertion/extraction". *Electrochemical and Solid-State Letters,* ***7***(5), pp. A93–A96.

[4] Tarascon, J. M., and Armand, M., 2001. "Issues and challenges facing rechargeable lithium batteries". *Nature,* ***414***(6861), pp. 359–367.

[5] Beaulieu, L. Y., Eberman, K. W., Turner, R. L., Krause, L. J., and Dahn, J. R., 2001. "Colossal reversible volume changes in lithium alloys". *Electrochemical and Solid-State Letters,* ***4***(9), pp. A137–A140.

[6] Yi, R., Dai, F., Gordin, M., Sohn, H., and Wang, D., 2013. "Influence of silicon nanoscale building blocks size and carbon coating on the performance of microsized sic composite liion anodes". *Advanced Energy Materials,* ***3***(11), pp. 1507–1515.

[7] Song, J., Chen, S., Zhou, M., Xu, T., Lv, D., Gordin, M., Long, T., Melnyk, M., and Wang, D., 2014. "Microsized siliconcarbon composites composed of carbon-coated sub-10 nm si primary particles as high-performance anode materials for lithium-ion batteries". *Journal of Materials Chemistry A,* ***2***(5), pp. 1257–1262.

[8] Sethuraman, V. A., Nguyen, A., Chon, M. J., Nadimpalli, S. P., Wang, H., Abraham, D. P., Bower, F., Shenoy, V. B., and Guduru, P. R., 2001. "Stress evolution in composite silicon electrodes during lithiation/delithiation". *Journal of The Electrochemical Society,* ***160***(4), pp. A739–A746.

[9] Sethuraman, V. A., Srinivasan, V., Bower, A., and Guduru, P., 2010. "In situ measurements of stress-potential coupling in lithiated silicon". *Journal of The Electrochemical Society,* ***157***(11), pp. A1253–A1261.

[10] Sethuraman, V. A., Chon, M. J., Shimshak, M., Srinivasan, V., and Guduru, P., 2010. "In situ measurements of stress evolution in silicon thin films during electrochemical lithiation and delithiation". *Journal of Power Sources,* ***195***(15), pp. 5062–5066.

[11] Larché, F. C., and Cahn, J. W., 1973. "A linear theory of thermochemical equilibrium of solids under stress". *Acta Metallurgica,* ***21***(8), pp. 1051–1063.

[12] Larché, F. C., and Cahn, J. W., 1978. "A nonlinear theory of thermochemical equilibrium of solids under stress". *Acta Metallurgica,* ***26***(1), pp. 53–60.

[13] Larché, F. C., and Cahn, J. W., 1982. "The effect of self-stress on diffusion in solids". *Acta Metallurgica,* ***30***(10), pp. 1835–1845.

[14] Tanim, T. R., Rahn, C. D., and Wang, C. Y., 2015. "A temperature dependent, single particle, lithium ion cell model including electrolyte diffusion". *Journal of Dynamic Systems, Measurement, and Control,* ***137***(1), p. 011005.

[15] Rahn, C. D., and Wang, C. Y., 2013. *Battery systems engineering*. John Wiley & Sons.

[16] Santhanagopalan, S., Guo, Q., Ramadass, P., and White, R., 2006. "Review of models for predicting the cycling performance of lithium ion batteries". *Journal of Power Sources,* ***156***(2), pp. 620–628.

[17] Zhang, X., Shyy, W., and Sastry, A. M., 2007. "Numerical simulation of intercalation-induced stress in li-ion battery electrode particles". *Journal of the Electrochemical Society,* ***154***(10), pp. A910–A916.

[18] Yao, Y., McDowell, M., Ryu, I., Wu, H., Liu, N., Hu, L., Nix, W., and Cui, Y., 2011. "Interconnected silicon hollow nanospheres for lithium-ion battery anodes with long cycle life". *Nano letters,* ***11***(7), pp. 2949–2954.

[19] Timoshenko, S., 1925. "Analysis of bi-metal thermostats". *Journal of the Optical Society of America,* ***11***(3), pp. 233–255.

[20] Chen, J., Liu, J., Qi, Y., Sun, T., and Li, X., 2013. "Unveiling the roles of binder in the mechanical integrity of electrodes for lithium-ion batteries". *Journal of The Electrochemical Society,* ***160***(9), pp. A1502–A1509.